surface area and high fraction of surface atoms.[1] Currently, Ag-NPs are the most commonly used nanomaterials, being used as antibiotic agents in textiles, medical devices (wound dressings),[2] and appliances such as refrigerators and washing machines.[3] However, understanding of Ag-NPs toxicity lags behind the applications for this technology. Inadequate identification of the potential hazards and the management of risks from exposures could lead to serious human health problems.[4]

Brain capillary endothelial cells cooperate with pericytes and astrocytes to generate the unique barrier properties of the blood–brain barrier (BBB), which is part of the neurovascular unit that plays a crucial role in safeguarding the brain from potentially harmful endogenous and exogenous substances circulating in the blood. The BBB, with its tight junctions (TJs) and efflux transporters, restricts the entry of most therapeutic agents.[5] A promising approach to overcome limited flux into the central nervous system (CNS) is the use of nanoparticles.[6] However, the risk from nanoparticles for the BBB and CNS still needs more investigations. In recent years, how Ag-NPs induce BBB dysfunction and neurotoxicity has been of particular interest, because Ag-NPs have been shown to enter the brain by crossing the BBB in vitro and in vivo.[7–10] Previous studies reported that intravenous or subcutaneous injection of Ag-NPs can induce BBB dysfunction, astrocyte swelling, and neuronal degeneration in rats.[7–9] The BBB permeability mechanisms of Ag-NPs were further investigated using an in vitro BBB model (cocultures of rat brain microvascular endothelial cells with astrocytes). The results showed that Ag-NPs crossed the BBB mainly by transcytosis rather than through the paracellular pathway.[10] Another study showed that Ag-NPs can increase BBB permeability and interact with the cerebral microvascular unit, producing a proinflammatory cascade that may further induce brain inflammation and neurotoxicity.[11] Most of the studies of Ag-NP-induced BBB dysfunction only focused on permeability changes and/or toxicity to the endothelial cells. However, brain microvascular endothelial cells cooperate with pericytes and astrocytes to generate the unique barrier properties of the BBB. The BBB is part of the neurovascular unit that plays a crucial role in safeguarding the brain from potentially harmful endogenous and exogenous compounds circulating in the blood.[5] A comprehensive understanding of how Ag-NPs induce BBB dysfunction and cause further toxicity and the mechanisms of action in brain endothelial cells, pericytes, and astrocytes remain largely unknown.

Ag-NPs encounter astrocytes immediately after crossing the BBB, because these brain cells almost completely cover the brain capillaries with their end feet.[12] Astrocytes are the most abundant cell type in the brain. They provide metabolic nutrients to neurons and protect the brain against oxidative stress and metal toxicity.[13,14] It is critical to understand how Ag-NPs affect astrocyte functions and induce potential toxicity. Recent studies showed that Ag-NPs accumulated in cultured astrocytes.[15–17] The accumulated Ag-NPs did not compromise the viability and the basal metabolism of cultured primary astrocytes. Ag-NPs induced upregulation of metallothioneins and heme oxygenase 1 to prevent silver-mediated toxicity, which could be induced by Ag-NP-derived Ag ions.[16] However, another study, using a mixed primary cell model consisting mainly of neurons and astrocytes and a minor proportion of oligodendrocytes, demonstrated that Ag-NPs induced oxidative stress and acute calcium responses. The Ag-NPs were mainly taken up by astrocytes, which changed astrocyte morphology, but not by neurons.[17] These contradicting results demonstrated that the effects of Ag-NPs on astrocytes remain uncertain. More studies are needed to comprehensively investigate the effects and toxicological mechanism(s) of Ag-NPs on astrocytes after they cross the BBB.

In this study, a triple coculture BBB model comprising microvascular endothelial cells, pericytes, and astrocytes was used to mimic the in vivo anatomical situation. The effects of Ag-NP suspension (Ag-NPS, containing silver nanoparticles and released silver ions) on BBB permeability and toxicity were studied. Polystyrene-NPs (PS-NPs) and Ag-NP-released Ag ions were studied to compare the toxic effects with respect to different raw chemical composition and/or form of silver. BBB permeability was studied after exposure to Ag-NPS and PS-NP. Ultrastructural changes of microvascular endothelial cells, pericytes, and astrocytes were observed by transmission electron microscopy (TEM). Then, DNA microarray was used to detect gene expression profiling of primary rat astrocytes in the triple coculture BBB model after exposure to Ag-NPS, the released Ag ions, and PS-NP. The mechanisms of Ag-NPS-induced toxicity on astrocytes were then evaluated using bioinformatics analyses, combined with observation of cellular morphological changes. Expressions of specific candidate genes were determined using real-time polymerase chain reaction (PCR). The results of this study provide comprehensive insight about Ag-NPS-induced toxicity on the biomimic BBB and the mechanism(s) of Ag-NPS-induced neurotoxicity on astrocytes, which will help us to have a better understanding of the importance of Ag-NPS-induced toxicity on astrocytes in the CNS.

Materials and methods

Characterization of materials

A Ag-NPS (2,000 μg/mL) was purchased from Nanux (SL1105001, Korea). PS-NP powder was purchased from Base Line Chrom Tech Research Centre (6-1-0005, People's Republic of China). The PS-NP powder was dispersed in sterile deionized water (2,000 μg/mL). The Ag-NP or PS-NP suspensions were then diluted with cell culture medium to the required final concentrations. The suspensions were sonicated (300 W, 42 kHz) in an icewater bath for 5 minutes before use. The Ag ion solution used in this study was prepared by incubating the Ag-NPS (10 μg/mL) for 24 hours at 37°C and then centrifuging it at 20,000 rpm for 2 hours. The total Ag contents before centrifugation and Ag ions contained in the supernatant after centrifugation were determined using atomic absorption spectrometry. This supernatant contained only the released Ag ion portion of the incubated Ag-NPS, which was used as the Ag ion solution treatment. The morphology, characteristics, surface charge, and crystallinity of Ag-NPS were observed by using TEM (HITACHI, Ibaraki, Japan), energy-dispersive X-ray spectroscopy (EDX; EDAX, USA), X-ray photoelectron spectrometry (XPS; ESCALAB250Xi, USA), and X-ray diffraction (XRD; D/MAXTTRIII; CBO, Japan), respectively. The size distribution of Ag-NPs and PS-NPs suspended in deionized water and the zeta-potential were determined using a Malvern Zeta Sizer Nano ZS (Malvern Instruments, Malvern, UK).

In vitro BBB model establishment

The primary rat microvascular endothelial cells, pericytes, and astrocytes were isolated and the in vitro biomimetic BBB was established as described in a previous study.[18] The animal work was approved by the Nagasaki University Institutional Animal Care and Use Committee. The primary rat cells were collected according to the guidelines in the use of animals in Japan. The details for cell isolation, cell culture, and characterization of cell purity are described in a previous study.[18] Briefly, pericytes were seeded in Transwell® membrane inverted cell culture inserts (1.12 cm^2 for a 12-well polycarbonate plate; Corning Incorporated, NY, USA). After 4 hours, primary brain endothelial cells were added to the luminal compartment of the inserts at a density of 2×10^6 cells/cm^2 having pericytes on the other side and positioned in the 12-well plates containing the astrocytes. The microvascular endothelial cells, pericytes, and astrocytes were cocultured in Dulbecco's Modified Eagle's Medium F-12 (with 10% fetal bovine plasma derived serum). From Day 2, cells were grown in culture media containing 500 nM hydrocortisone. Experiments were performed on Day 5. Transendothelial electrical resistance (TEER) was measured at days 2, 4, and 5 using a Millicell-ERS2 (Millipore, Billerica, MA, USA). Experiments were performed when TEER was >200 Ω·cm^2. Previous research demonstrated that in vitro BBB models with TEER >150 Ω·cm^2 give reasonable drug permeability results.[19–21]

Cell treatments

Ag-NPS (1 μg/mL and 10 μg/mL) and PS-NPs (100 μg/mL) were introduced into the Transwell® lumen at Day 5 of BBB model culture. After 24-hour treatment, TEER was measured using a Millicell-ERS2, and the Transwell® membrane (with microvascular endothelial cells and pericytes) and astrocytes were washed three times and cells were collected for confocal microscopy or TEM, respectively. These experiments were performed in triplicate wells.

For the DNA microarray experiment, Ag-NPS (10 μg/mL), Ag ions released from 10 μg/mL of Ag-NPS, and PS-NPs (100 μg/mL) were introduced into the Transwell® lumen. After 24 hours, astrocytes were collected for DNA microarray analysis. Briefly, astrocytes were washed three times using PBS, then digested with trypsin, and collected in Trizol solution for RNA extraction.

TEM and immunostaining

The Transwell® BBB model was exposed to Ag-NPS and PS-NPs for the concentrations and time durations indicated earlier. The Transwell® membrane and astrocytes were collected for TEM and immunostaining, respectively. The details of TEM were described in our previous study.[22] A certified pathologist identified different cell organelles and Ag-NPs were identified according to their high density under TEM. For Confocal laser scanning microscopy of ZO-1 immunostaining, the secondary antibodies Alexa Fluor 488 conjugated anti-mouse immunoglobulins (Invitrogen, CA, USA) were used in a dilution 1:1000. To counter stain cell nuclei TO-PRO-3 Iodide (Invitrogen Corporation, CA, USA) was used in a dilution of 1:300. The immunostaining of the TJ protein ZO-1 was examined by a LSM5 PASCAL Zeiss confocal laser scanning microscope (Leica, Japan).

Total RNA isolation and DNA microarray

Total RNA was extracted from the collected astrocytes using the RNeasy reagent and the mini protocol for isolation of total RNA from animal cells (QIAGEN, Tokyo, Japan) according to the instructions provided by the manufacturer. The experimental details were described in our previous study.[22] The DNA microarray experiment was conducted using Agilent

G4130F Whole Rat Genome Microarray 4×44 K (Agilent, CA, US). To determine biologically relevant gene ontology (GO) terms (provided by the National Center for Biotechnology Information) of differentially expressed genes, the software "PANTHER" was used. It provides gene expression data analysis/comparison of gene lists (http://www.pantherdb.org/tools/genexAnalysis.jsp). The analysis was performed using Unigene ID as the identifier for biological process categories.

Quantitative real-time PCR

Quantitative real-time PCR (SYBR Green method) for five selected genes ("test" genes) was performed to determine their gene expression levels and to verify the reliability of the microarray data. Primers used in this study are listed in Table 1. The details of the method were described in our previous study.[22]

Results

Ag-NP characterization

The characterization of Ag-NPs used in this study was described in our previous study.[23] The morphology of Ag-NPs in distilled water was observed using TEM (Figure 1A). The particle size distribution in distilled water was 7±2 nm. The zeta potential was −37.8±3.2 mV in water. In cell culture medium, the particle size distribution was 101±12 nm and the zeta potential was −7.9±0.6 mV. The XRD pattern of the Ag-NP showed the typical nature of the Ag-NP (data not shown). EDX results confirmed the presence of silver in cell culture medium (Figure 1B) and XPS results showed both Ag^0 (81%) and Ag^+ (19%) in the deposits of Ag-NPS diluted with cell culture media (Figure 1C), indicating that both Ag-NPs and Ag ions exist in the Ag-NPS. The silver ion content contained in 10 μg/mL of Ag-NPS (incubated for 24 hours, at 37°C) occupied 1.1% of the total silver contents. The particle size distributions of PS-NPs in water and cell culture medium were 33±8 nm and 35±8 nm, respectively. The zeta potentials of PS-NPs in water and cell culture medium were −29.6±2.6 mV and −8.93±0.16 mV, respectively.

Characterization of isolated primary cells

Primarily isolated rat brain microvascular endothelial cells grew into continuous monolayers and showed tightly arranged, nonoverlapping, elongated, and fusiform morphology. Microvascular endothelial cells were strongly positively immunostained for Factor VIII, an endothelial marker, indicating high purity of endothelial cells. Expression of TJ proteins, such as ZO-1 and Claudin-5, was observed by confocal microscopy, indicating the properties of BBB cells (Figure 2A). Astrocytes were polygonal with long cell processes, resembling astrocyte end feet, and strongly positive for glial fibrillary acidic protein staining (Figure 2B). Pericytes in culture spread large with irregular projections. The cells described herein were used to establish the in vitro BBB model. A schematic drawing of the in vitro BBB model is shown in Figure 3. Experiments were carried out on Day 5 when the TEER values of the BBB model were >200 $\Omega \cdot cm^2$.

Effect of Ag-NPS and PS-NPs on the TJ of the BBB

The TEER values of the BBB in vitro model were all >200 $\Omega \cdot cm^2$ before the experiment (Figure 4A). After 24-hour treatments, the PS-NP and Ag-NPS (1 μg/mL) groups did not change their TEER values significantly compared to control. However, the 10 μg/mL Ag-NPS group showed significantly decreased TEER values compared to control (Figure 4B). The immunostaining of the TJ protein ZO-1 of microvascular endothelial cells in the coculture BBB model showed a continuous, smooth, pericellular, belt-like pattern in the control and PS-NP groups. However, ZO-1 expression was apparently decreased in the 10 μg/mL Ag-NPS group compared to control (Figure 5), which was consistent with the TEER results.

Table 1 Primers used in the present study for real-time polymerase chain reaction

Gene	GeneBank	Primary sequence 5′–3′
Txnip	NM_001008767	Forward primer: GGAGAAAGTTCTGCTCTCG
		Reverse primer: AAGTGCTAAGGCGGAGTAA
Ddit4	NM_080906	Forward primer: TAACACCAGGGAGCTGC
		Reverse primer: ACAGTTCACTCCTCCAGTACA
Nr4a1	NM_024388	Forward primer: ATCTCTTCCGCTCTCCT
		Reverse primer: ATCAGAATCTGTCAATCACCT
Egr2	NM_053633	Forward primer: TTATTAGCTCTTAATAGTTGTGGAAA
		Reverse primer: CTGAACTCCAGTTAGTGGT
Fos	NM_022197	Forward primer: GGGAGGACCTTATCTGTGC
		Reverse primer: GGATGCTTTCAAGTCCTTGAG

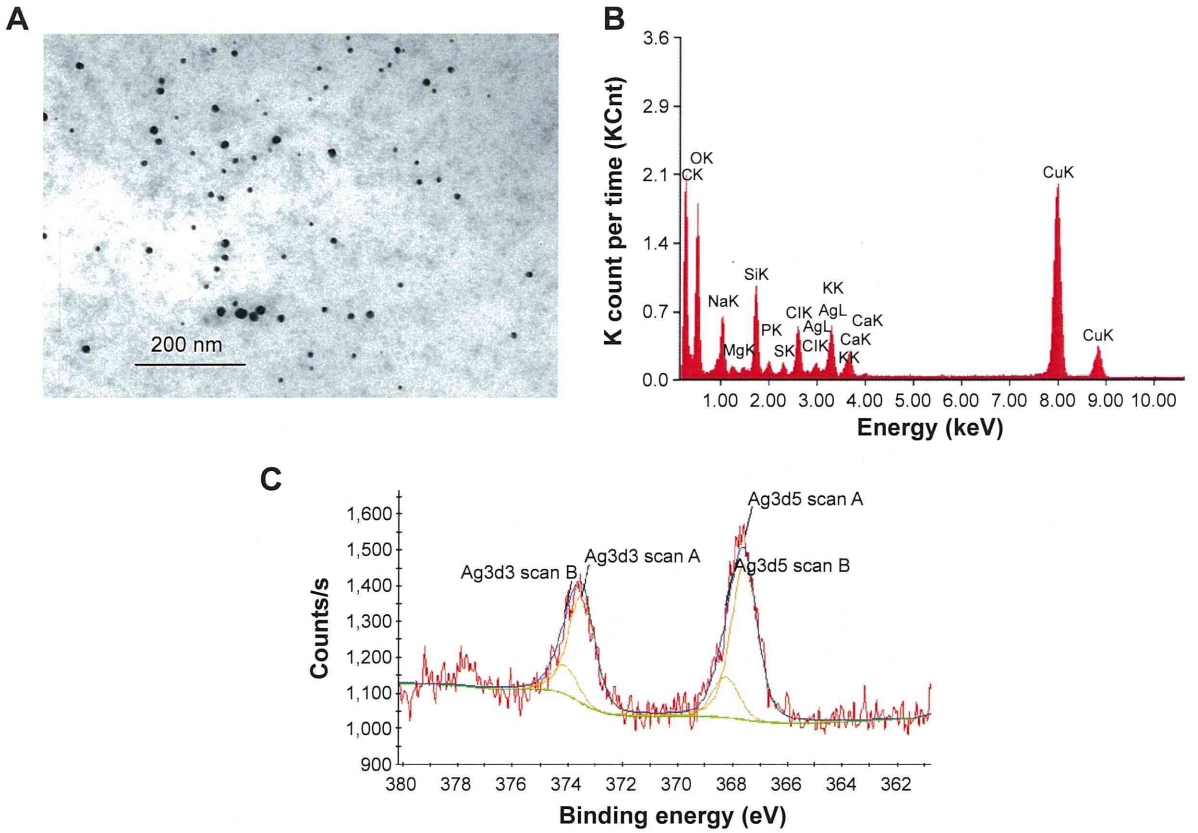

Figure 1 Characterization of Ag-NP.
Notes: (**A**) TEM image of Ag-NPs in distilled water. (**B**) EDX of Ag-NPS in cell culture media. (**C**) XPS analysis of Ag-NPS in cell culture media. The experiments were performed by using the deposits of Ag-NP/cell culture medium suspension.
Abbreviations: Ag-NP, silver nanoparticle; Ag-NPS, Ag-NP suspension; EDX, energy-dispersive X-ray spectroscopy; TEM, transmission electron microscopy; XPS, X-ray photoelectron spectrometry.

Effects of Ag-NPS and PS-NPs on the ultrastructural changes of the BBB

TEM images showed that microvascular endothelial cells formed the TJs very well in the in vitro BBB model (Figure 6Aa), and pericytes spread large with irregular projections on the other sides of the Transwell® membrane in the control group (Figure 6Ba). In PS-NP group, no significant TJ disruptions were observed between microvascular endothelial cells (Figure 6Ab). No ultrastructural changes were observed in the pericytes (Figure 6Bb). In the 1 μg/mL Ag-NPS group, discontinuous TJs were not observed. Vacuolations and endoplasmic reticulum (ER) expansion were occasionally observed in the microvascular endothelial cells (Figure 6Ac and d). Vacuolations were also occasionally observed in pericytes (Figure 6Bc). In the 10 μg/mL Ag-NPS group, Ag-NP-like nanoparticles were observed inside the endothelial cells and pericytes. Apart from discontinuous TJ, ER expansion, vacuolations, and mitochondrial shrinkage were also observed (Figure 6Ae and f). Vacuolations were observed in pericytes in the 10 μg/mL Ag-NPS group (Figure 6Bd).

Effects of Ag-NPS on the ultrastructural changes of astrocytes

Astrocytes did not show significant cytotoxicity, such as morphological changes and damages in all treatment groups compared to the control, as observed by light microscopy (data not shown). TEM images showed that astrocytes grew with normal morphology in the control group (Figure 6Ba). In the PS-NP and 1 μg/mL Ag-NPS groups, no ultrastructural changes were observed in astrocytes in most images, and mitochondrial shrinkage was observed occasionally (Figure 6Bb and c). In the 10 μg/mL Ag-NPS group, severe mitochondrial shrinkage was observed (Figure 6Bd) and nuclear atypia was observed occasionally (Figure 6Be). Meanwhile, Ag-NP-like particles appeared inside astrocytes (Figure 6Bf).

Global gene expression changes

Filtering of the array results was done for astrocytes as follows: genes were considered to be upregulated or downregulated when the relative expression levels [Log_2(gene expression ratio of treated/control)] differed by >1 or less

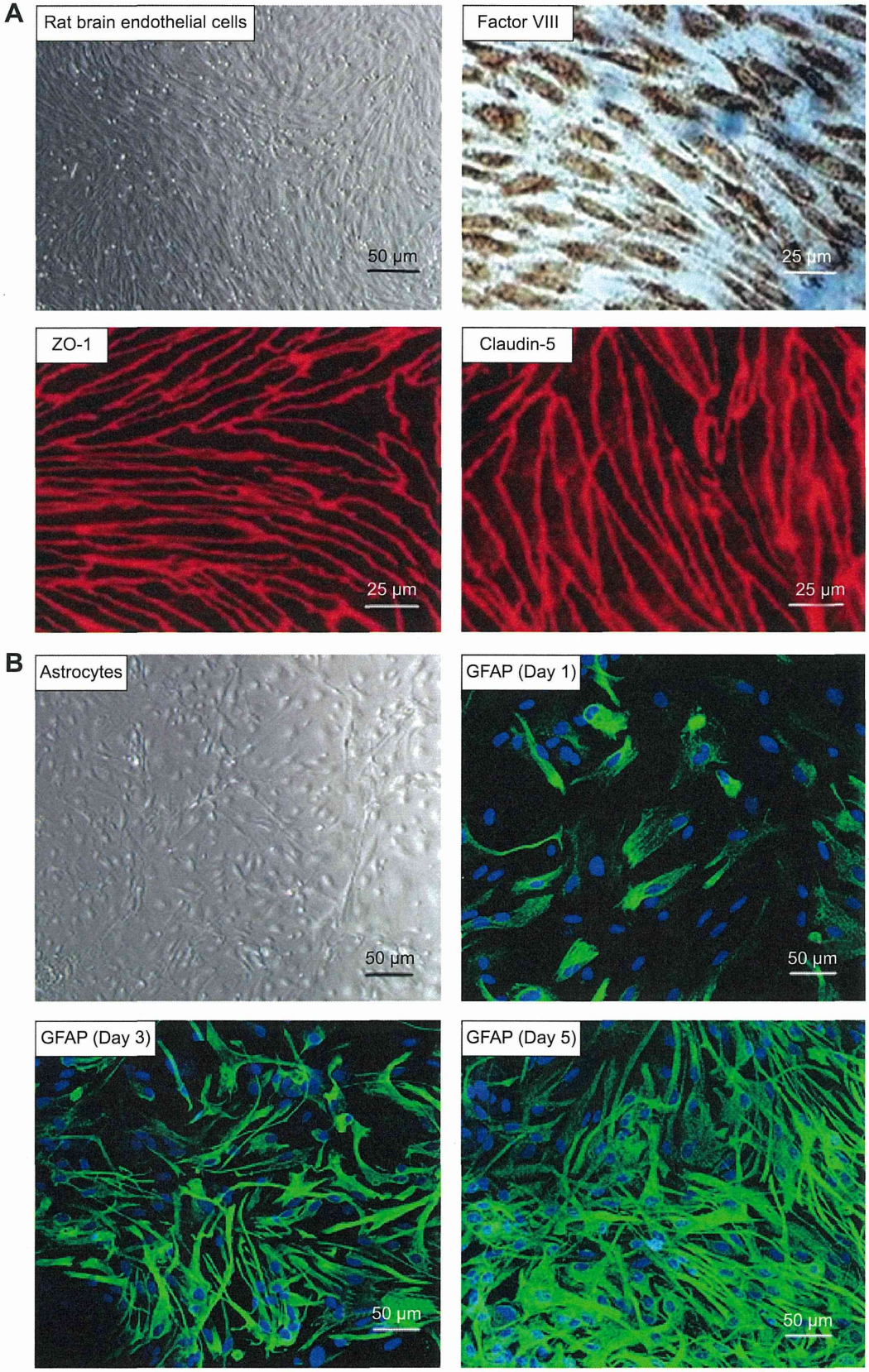

Figure 2 Characterization of primary rat brain microvascular endothelial cells.
Notes: (**A**) Primary rat brain microvascular endothelial cells form a pure, near-confluent monolayer by light microscopy (upper left panel). Factor VIII (a marker for endothelium; red), ZO-1, and Claudin-5 (tight junction proteins; red) expressions are positive in primary rat brain microvascular endothelial cells by confocal microscopy. (**B**) Characterization of primary astrocyte cultures in different confluence culture condition by light microscopy (upper left panel) and confocal microscopy. Astrocytes are positive for GFAP.
Abbreviation: GFAP, glial fibrillary acidic protein.

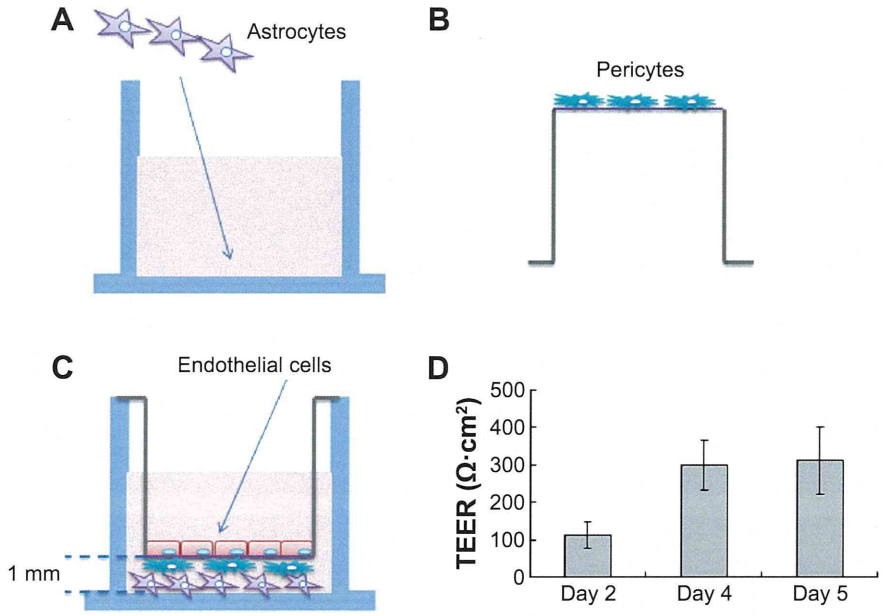

Figure 3 Schematic drawing of the preparation of the in vitro blood–brain barrier model.
Notes: (**A**) Rat astrocytes were seeded at the bottom of 12-well plates, while (**B**) rat brain pericytes were seeded at the against-lumen side of Transwell® membranes of inverted cell culture inserts. After 4 hours, (**C**) endothelial cells were seeded into the luminal compartment of the inserts having pericytes on the other side and positioned into the 12-well plates containing the astrocytes. (**D**) TEER (expressed as Ω·cm²) of the blood–brain barrier model, measured on different days. Data are presented as mean ± SD (n=3).
Abbreviations: SD, standard deviation; TEER, transendothelial electrical resistance.

than −1 in treated groups (10 μg/mL Ag-NPS or released Ag ion or 100 μg/mL PS-NP) compared to control. We observed that 23 genes in total were differentially expressed in the 10 μg/mL Ag-NPS-treated group compared to control. Of the 23 genes, there were 20 downregulated genes and 3 upregulated genes in astrocytes (Table S1). Sixteen genes in total were differentially expressed in the released Ag ion-treated group compared to control, and there were 15 downregulated genes and 1 upregulated gene (Table S2).

By comparing the gene expression profiles of astrocytes exposed to Ag-NPS or their released Ag ions (Tables S1A, S1B, S2A, and S2B), we observed a total of nine genes (eight genes downregulated and one gene upregulated) that were changed in common, suggesting that changes in these genes are attributable to the released Ag ions. This implies that 2 genes from the total of 3 upregulated genes and 12 genes from the total of 28 downregulated genes were uniquely induced by Ag-NPs, not released Ag ions. Furthermore, the upregulated genes in common showed a higher expression level in the Ag-NPS treatment group than in the released Ag ion group. The downregulated genes (nuclear receptor subfamily 4, group A, member 1 [*Nr4a1*], early growth response 2 [*Egr2*], protein kinase KID2 [*kid2*], nuclear receptor subfamily 4, group A, member 3 [*Nr4a3*], and

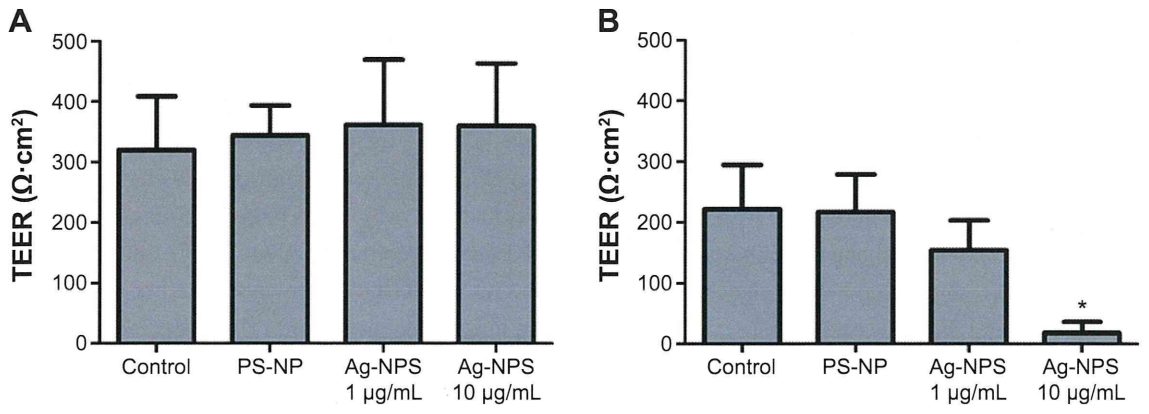

Figure 4 The effect of Ag-NPS and PS-NP on BBB permeability measured by TEER.
Notes: TEER (expressed as Ω·cm²) of the BBB model (**A**) before and (**B**) after 24 hours' treatment in control, PS-NP (100 μg/mL), and Ag-NPS (1 μg/mL and 10 μg/mL) groups. All data are presented as mean ± SD. *Significant difference compared to the control ($P<0.05$).
Abbreviations: Ag-NPS, silver nanoparticle suspension; BBB, blood–brain barrier; PS-NP, polystyrene nanoparticle; SD, standard deviation; TEER, transendothelial electrical resistance.

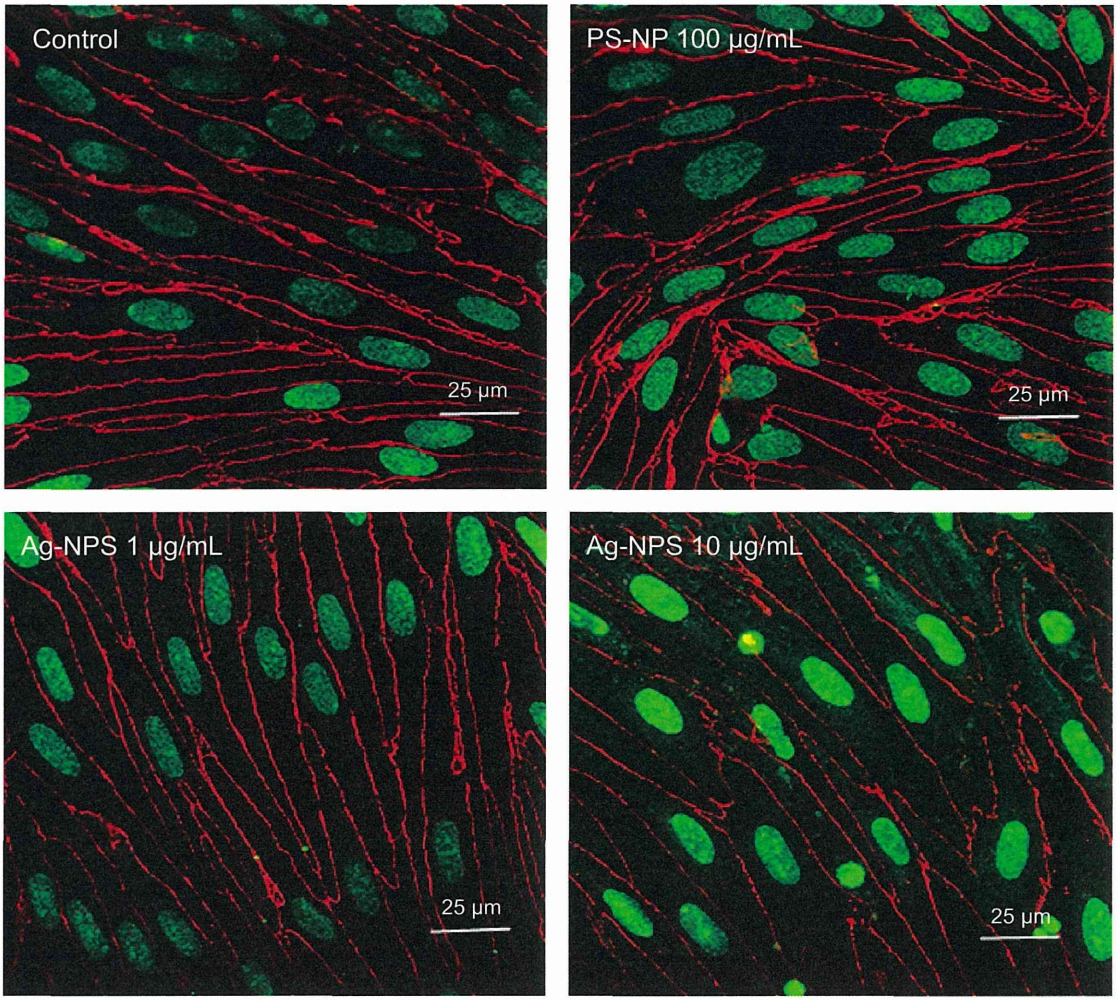

Figure 5 Immunofluorescent staining of tight junction protein ZO-1 (red) in confluent brain endothelial cell in triple coculture.
Notes: The ZO-1 immunostaining of endothelial cells in coculture shows a continuous, smooth, pericellular, belt-like pattern in control and PS-NP groups. However, ZO-1 immunostaining was significantly decreased in the 10 μg/mL Ag-NPS group compared to the control.
Abbreviations: Ag-NPS, silver nanoparticle suspension; PS-NP, polystyrene nanoparticle.

activity-regulated cytoskeleton-associated protein [*Arc*]) showed a greater extent of decreases in the Ag-NPS group compared with the levels in the released Ag ion group. The other three downregulated genes (protein sprouty homolog 1 [*spry1*], dual specificity phosphatase 5 [*Dusp5*], and chemokine (C–X–C motif) ligand 1 [*Cxcl1*]) have similar changes in both Ag-NPS and Ag ion groups. These results indicate that the toxic responses observed in Ag-NPS-exposed astrocytes are attributable to both Ag-NPs and their released Ag ions. Ag-NPS caused higher gene expression changes compared with their released Ag ion group, suggesting a synergistic toxic effect induced by Ag-NPS and their released Ag ions.

Pathway analysis

To further investigate the molecular mechanism of Ag-NPS-induced cellular responses, GO and Kyoto Encyclopedia of Genes and Genomes (KEGG) molecular pathway analyses were performed. In the 10 μg/mL Ag-NPS-treated group, 139 biological functions were changed based on GO (Table S3), which were associated with metabolic processes, biosynthetic processes, response to stimuli stimulus, developmental processes, regulation of molecular function, biological processes, transcription, regulation of signaling, cell death, gene expression, learning, memory, and behavior (Figure 7). The MAPK signaling pathway was significantly changed in KEGG pathway analysis, which was linked to four genes (*Dusp1*, *Dusp5*, FBJ osteosarcoma oncogene [*Fos*], and *Nr4a1*). However, no GO and KEGG pathways were changed in the released Ag ion-treated group and PS-NP-treated group.

Quantitative real-time PCR determination

To determine the gene expression level and verify the reliability of differentially expressed genes identified by the

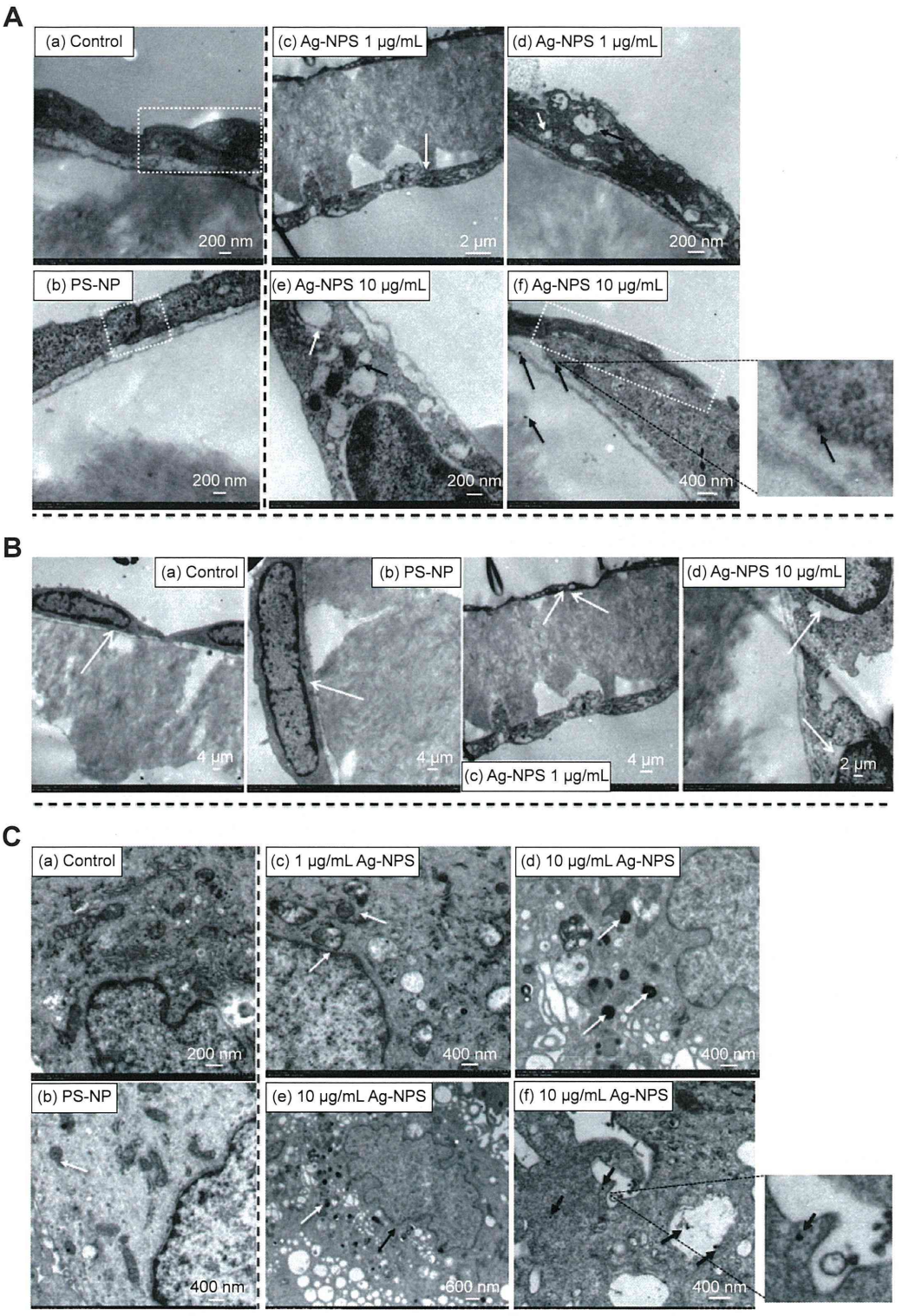

Figure 6 TEM images of primary rat brain (**A**) microvascular endothelial cells, (**B**) pericytes, and (**C**) astrocytes after 24-hour treatments.

Notes: (**A**) In the control group, endothelial cells form TJs (a, white dash box). In the PS-NP group, a TJ (b, white dash box) between endothelial cells was not disrupted. In the 1 μg/mL Ag-NPS group, the endothelial cells grew nicely on the membrane (c, white arrow) and discontinuous TJs were not observed. Vacuolations (d, white arrow) and ER expansion (d, dark arrow) were observed in the endothelial cells. In the 10 μg/mL Ag-NPS group, mitochondrial shrinkage (e, dark arrow) and ER expansion (e, white arrow) appeared; Discontinuous TJs (f, white dash box) and Ag-NP-like particles as showed in the insert for (f) (f, dark arrows) in endothelial cells were observed. (**B**) Pericytes grew nicely on the other side of the membrane (white arrow) in the control group (a) and PS-NP group (b). In the 1 μg/mL Ag-NPS group, vacuolations (white arrows) were observed occasionally in pericytes (c). In the 10 μg/mL Ag-NPS group, vacuolations (white arrows) were observed in pericytes (d). (**C**) In the control group, astrocytes had normal cell morphology (a). In the PS-NP group, mitochondrial shrinkage was observed occasionally (white arrow) (b). In the 1 μg/mL Ag-NPS group, mitochondrial shrinkage was occasionally observed (white arrows) (c). In the 10 μg/mL Ag-NPS group, nuclear atypia (black arrows) and severe mitochondrial shrinkage (white arrows) were observed (d and e); Ag-NP-like particles (showed in the insert for f) were also observed in astrocytes (f, black arrows), as well as in the enlarged picture.

Abbreviations: Ag-NPS, silver nanoparticle suspension; ER, endoplasmic reticulum; PS-NP, polystyrene nanoparticle; TEM, transmission electron microscopy; TJ, tight junction.

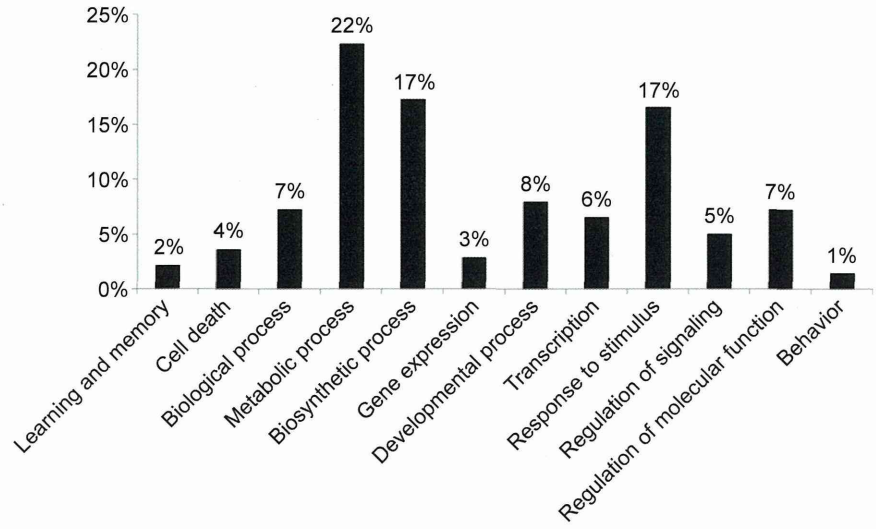

Figure 7 *Functional classification (GO terms) of differentially expressed genes based on GO.*
Notes: The data were collected from astrocytes exposed to 10 μg/mL of Ag-NPS for 24 hours. The percentage of related GO terms for each category is indicated. Percentage (%) = (related GO terms for each category/related GO terms for all categories) ×100%.
Abbreviations: Ag-NPS, silver nanoparticle suspension; GO, gene ontology.

DNA microarray, five genes selected from the groups of up- and downregulated genes after exposure to Ag-NPS and released Ag ions were further examined using quantitative real-time PCR. Thioredoxin interacting protein-encoding gene (*Txnip*) and DNA damage inducible transcript 4 (*Ddit4*) were upregulated, while *Nr4a1*, *Egr2*, and *Fos* were downregulated in both reverse transcriptase-PCR and DNA microarray (Table 2).

Discussion

Nanoparticles have been increasingly used in medicine, cosmetics, electronics, and food additives. However, the influence of nanoparticles on human health and brain has not been studied well.[24] Several studies have demonstrated that Ag-NPs can enter the CNS[25] and induce brain edema and neurotoxicity.[10,11,26–29] Our previous studies showed that Ag-NPS and/or released Ag ions crossed the BBB and subsequently caused damage to astrocytes and neurons.[23] Cadherin and claudin expression were slightly changed in the Ag-NPS-exposure group, and astrocyte swelling was the most significant change after a 2-week gastrointestinal exposure to 1 mg/kg or 10 mg/kg of Ag-NPS in rats. Furthermore, Ag-NPs interacting with the cerebral microvasculature can induce formation of reactive oxygen species (ROS) and proinflammatory mediators, which can increase BBB permeability.[7–9,11] However, the biological effects of Ag-NPs on the BBB and brain are still unclear. It is critical to further understand the toxicity of Ag-NPS using a biomimic BBB model. In the present study, we demonstrated for the first time the toxic responses and mechanisms of Ag-NPS by observing the ultrastructure and gene expression profile changes using a biomimetic BBB model (microvascular endothelial cells/pericytes/astrocytes).

In the current study, we established a primary BBB triple coculture model. The model used primary rat brain microvascular endothelial cells, pericytes, and astrocytes corresponding to the anatomical situation in brain capillaries. Previous research showed that pericytes contributed to the

Table 2 RT-PCR validation of selected genes from microarray data

Gene	Ag-NPS		Ag ion	
	RT-PCR (mean ± SE)*	Microarray (Log_2)#	RT-PCR (mean ± SE)*	Microarray (Log_2)#
Txnip	4.20±0.16	1.836	2.32±0.10	1.109
Ddit4	2.87±0.15	1.581	1.94±0.12	0.883
Nr4a1	0.03±0.00	−3.463	0.35±0.14	−1.982
Egr2	0.08±0.01	−2.898	0.43±0.12	−1.292
Fos	0.29±0.02	−1.462	0.97±0.13	−0.192

Notes: *Mean ± SE; experiment was performed in triplicate; #Log_2 = Log_2 (gene expression ratio of Ag-NPS or Ag ion/Control).
Abbreviations: Ag-NPS, Ag-NP suspension; RT-PCR, reverse transcriptase polymerase chain reaction; SE, standard error.

maturation and maintenance of BBB properties[30] and there was a clear correlation between a higher ratio of pericytes versus endothelial cells in blood vessels and the tightness of the endothelial barrier.[31] Furthermore, astrocytes can decrease the paracellular permeability of immortalized rat brain endothelial cells.[32] In the present study, the high expression of TJ proteins and the high TEER demonstrated that the triple coculture model is among the best primary BBB models to mimic the BBB in vivo.[33] This primary BBB model provides a very useful in vitro model to evaluate the effect of vasculotoxic or vasculoprotective agents on the BBB. In this study, this triple coculture model was used to investigate the changes to BBB integrity and the molecular mechanisms in vitro following exposure to Ag-NPS.

As mentioned herein, several studies showed that Ag-NPs can disrupt the BBB and cause CNS toxicity. However, the toxicological effects of Ag-NPs on the typical biomimetic BBB are still uncertain. In the present study, 10 μg/mL Ag-NPS showed significant effects on BBB permeability and TJ protein expression, whereas 1 μg/mL Ag-NPS did not. Vacuolations were also observed by TEM in pericytes after Ag-NPS exposure. Previous studies demonstrated that pericyte deficiency or dysfunction leads to chronic BBB damage and contributes to neurodegeneration during Alzheimer's disease pathogenesis.[34–36] Further studies are needed to investigate whether Ag-NPS can cause pericyte dysfunction and potential neuronal injury. We further observed a large amount of mitochondrial shrinkage and ER extension, as well as Ag-NP-like particles, in astrocytes by TEM, which demonstrated that Ag-NPs entered astrocytes and induced toxicity after crossing the endothelial cells and pericytes.

To identify the molecular mechanisms of multiple genes working together following exposure to Ag-NPS, released Ag ions, and PS-NPs, microarray assays of astrocytes were performed to establish a global gene expression profile. The functional classification of these genes was analyzed using GO. Our results demonstrated that the toxicological effects on astrocytes were significantly different between the Ag-NPS and the released Ag ion or PS-NP group. In contrast with the Ag-NPS-treated group that showed induction of 139 GO and 1 KEGG pathway genes, no GO term and KEGG pathway gene was changed in the released-ion or PS-NP exposure group. The expression levels of 16 genes were changed after exposure to released Ag ions, but the fold changes were less in general compared with the changes in the Ag-NPS treatment group (Table S3). The results were consistent with our previous research, which showed that Ag-NPS induced greater toxicity compared with the released Ag ions. The greater toxicity was attributed to the Ag-NPS. Ag-NPs, as heavy metal nanoparticles, but not the characteristics of a nano-sized particle themselves (as do PS-NP), caused severe toxicity in astrocytes.

Ag-NPs have been demonstrated to induce oxidative stress and apoptosis in the brain.[37] The effects of 25 nm Ag-NPs on gene expression were evaluated in different regions of the mouse brain. Ag-NPs produced apoptosis and neurotoxicity by generating free radical-induced oxidative stress. The oxidative stress induced by Ag-NPs in the brain was also related to reduction of antioxidant capacity. Ag-NPs altered expression of genes such as *Txnip*, which is a member of the α-arrestin family involved in redox sensing and metabolic control.[38] Our data in Tables S1 and S2 obtained from real-time PCR showed that *Txnip* was significantly upregulated 4.20-fold and 2.32-fold in the Ag-NPS and Ag ion treatment groups, respectively. Upregulation of Txnip modulates antioxidant defense by inhibiting the Trx system and increasing ROS and oxidative stress.[39] Txnip also upregulated the transcription factor NF-κB, which induces transcription of proinflammatory cytokines such as tumor necrosis factor-α and interleukin-1β.[40] These two pathways can further activate the apoptotic MAPK pathway, leading to cell death.[41] Ag-NPs also activated the p38 MAPK pathway, causing apoptosis of Jurkat T cells.[42] In the present study, Ag-NPS also induced *Ddit4* expression. This was not produced by the released Ag ions. Ddit4 is known to inhibit mTOR activity, resulting in an increase in apoptosis in mouse embryonic fibroblasts.[43] Ddit4 can reduce cell proliferation, growth, and maturation by inhibiting mTOR-mediated synthesis of proteins.[44] Furthermore, in our study, five functional GO molecule annotations (nine genes) were involved in apoptosis/cell death only after Ag-NPS exposure. For example, *Nr4a1*, encoding an orphan nuclear receptor for neural apoptosis, was the most downregulated gene in astrocytes. *Nr4a1* has been implicated in apoptosis,[45] cell survival, and metabolism.[46] *Nr4a1* can be induced after excitotoxic and oxidative stress in neurons, and it upregulates neuroprotective genes and increases neuronal survival. *Nr4a1* also has early protective function in neural cells/tissues against various pathophysiological stresses.[47] In this study, Ag-NPS induced downregulation of *Nr4a1* in the astrocyte, which could decrease the neuroprotective function against oxidative stress. Ag-NPS exposure also reduced B-cell lymphoma 2 (*Bcl-2*) expression, which is present in the inner mitochondrial membrane and plays an important role in regulation of ROS production and apoptosis. A previous study showed that oxidative stress reduced *Bcl-2*